Bubble Sizing by Interferometric Laser Imaging

Yuzuru Niwa, Yoshihiro Kamiya, Tatsuya Kawaguchi and Masanobu Maeda

Department of System Design Engineering, Keio University

Hiyoshi 3-14-1 Kohoku-ku Yokohama Kanagawa 223-8522, Japan

Abstract

The objective of the present contribution is to establish a novel measurement technique for velocity and diameter of transparent spherical gas bubbles in order to obtain such important information as mass transfer rate at the interface of gas-liquid phases, or drag coefficient of the rising bubbles in liquid. This technique gives spatial distribution of velocity and diameter of bubbles simultaneously by capturing the sequential images of fringes by using a pulsed Nd:YAG laser source and a high resolution CCD camera. Figure 1 is a snapshot of the circular interferometric pattern generated by external reflection(p_0) and direct refraction(p_1) lights from the transparent spherical bubble from a nozzle of 60μm in diameter. This figure shows the difference of the diameter by counting the number of fringes or fringe spacing. Additionally, continuous acquisition of the image sequence enables us to know the velocity of individual bubbles by tracking their movement. Figure 2 illustrates the simplified experimental setup for the rising bubbles, including the flow field and optical equipment. The results of the gas dissolution measurement of spherical CO_2 bubbles into a stationary fluid show a range of measured bubble diameters of approximately 100μm to 1000μm with rising velocities up to 30mm/s.

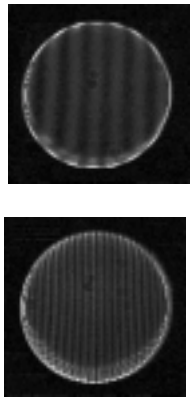

Figure 1: *Comparison of the fringe images of bubbles of different diameter.*

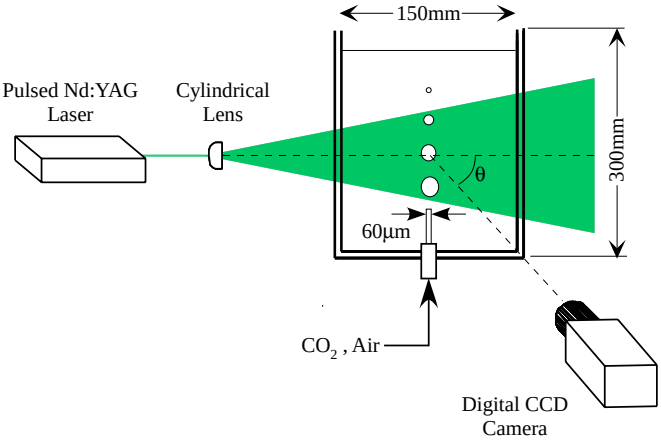

Figure 2: *Experimental Setup for observing the dissolution of the rising CO_2 bubbles into water.*

1 Introduction

Experimental investigations of gas-liquid two phase flow including droplets or gas bubbles are necessary to understand the behavior of droplets or bubbles in turbulence, and to evaluate the heat and mass transportation at the interface of the gas-liquid phases. For flow fields with large bubbles, whose diameters are more than 1mm, the shape of bubble becomes obviously elliptical as the Reynolds number and Eötvös number increase. There are many studies concerning bubbly flow which analyze the dynamic interaction between the three-dimensional deformation of bubbles and the surrounding flow in turbulence and shear flow[Brücker 1998; Ford *et al.*, 2000].

However, flow fields with small bubbles less than 1mm in diameter, whose shapes are almost spherical, are important for industrial applications including the reduction of greenhouse gas into seawater[Hirai *et al.*, 1997]. The measurement techniques that provide the information about the individual properties of droplets or bubbles are especially necessary in order to know the detailed behavior of them and to evaluate the heat and mass exchange at the interface of the phases; e.g. measurement techniques for the diameter of droplets[Durst *et al.*, 1975], temperature[Schaller *et al.*, 1994], refractive index[Lin *et al.*, 2000] and Shadow Doppler Velocimeter which is a diagnostic instrument for non-spherical and non-transparent particles[Morikita *et al.*, 1994]. The point measurement techniques, however, have a difficulty in resolving the spatial distribution of physical properties in a flow field such as; velocity, temperature and diameter.

The Interferometric Laser Imaging for Droplet Sizing(ILIDS) has been developed to measure the size of transparent spherical droplets[Roth *et al.*, 1993; Glover *et al.*, 1995; Girasole *et al.*, 1998; Hess, 1998; Pajot *et al.*, 1998]. The aforementioned researchers demonstrated the possibility of recording the size information of individual droplets into the instantaneous image of circular fringes, while Phase Doppler Anemometry can measure the diameter by noting the phase differences between the Doppler signals. The fundamental principle of the proposed technique was based on Mie Scattering theory and developed by an approach similar to ILIDS by considering the difference of a beam couple passing through the bubble. Since the focused image shows a couple of small spots that are reflective and refractive lights, the diameter of larger particle is determined from the distance of the two spots[Van de Hulst *et al.*, 1991]. However, it becomes difficult with smaller bubbles to obtain the entire information of the flow field due to the limitation of the magnification of the optical system and the pixel resolution of a CCD camera. In the case of capturing in the defocused plane, the size of the two spots are expanded and overlap with each other because the shape of the point-spread function of the spot illuminant through a lens is circular. Finally, the parallel fringe will appear in the overlapped area as shown in Figure 1 and we can observe the characteristic interfering pattern with a far-field arrangement of receiving optics. Moreover, an improvement was performed which provided the velocity of individual bubbles by using a cross correlation method in the double exposed images by pulsed laser illuminations.

The principle of the interferometric imaging technique and its application to the spherical bubble measurement are described in Section 2.1. The image processing method to extract the individual diameter and velocity from the circular fringe images is in Section 2.2, which is followed by the experimental results in Section 3 and conclusions in Section 4.

2 Principle

2.1 Interferometric Laser Imaging

ILIDS is a method that observes the interference of a couple of scattering lights from a single droplet. The approach of the proposed technique was similar to droplet measurement by considering the difference of a beam couple passing through the spherical bubble. Figure 3 illustrates the route of the beams at scattering angle, θ. The interferometric image as shown in Figure 1 is generated by the scattered lights of external reflection, p_0, and direct refraction, p_1, of droplets illuminated by a coherent laser source. The diameter is obtained by counting the number of fringes or fringe spacing. When the illumination is perfectly homogeneous, the intensity of these two scattered rays are much stronger than that of p_2 refraction and the others. The intensity of p_0 and p_1 rays are almost equal at the scattering angle $\theta = 45^\circ$ and the amplitude of interference is maximum, while the optimum angle for droplets is equal to $\theta = 68^\circ$. Figure 4 shows the calculation result given by Mie Scattering theory which represents the spatial distribution of the scattered light intensity from a single spherical bubble with $100\mu m$ diameter illuminated by a polarized broad laser source.

Firstly, we should illustrate that the relation between the number of fringes or fringe spacing and the diameter of bubble. Using Snell's law we can relate τ_0 and $\tau_1^{'}$ the incident angles of the external reflection and direct refraction rays, respectively.

$$\cos \tau_1^{'} = m \cos \tau_1 \tag{1}$$

Assuming that only two rays come from the bubble, their phase difference is derived from geometric analysis.

$$\begin{aligned} \delta_0 - \delta_1 &= \frac{2\pi d}{\lambda}\left(m \sin \tau_1 - \sin \tau_1^{'} - m \sin \tau_0\right) \\ &= \frac{2\pi d}{\lambda}\left(\sqrt{m^2 - 2m\cos(\theta/2) + 1} - m \sin(\theta/2)\right) \end{aligned} \tag{2}$$

The relation between phase difference $\Delta(\delta_1 - \delta_1)$ and angular difference $\Delta\theta$ is;

$$|\Delta(\delta_0 - \delta_1)| = \left| \frac{m\pi d}{\lambda}\left(\frac{\sin(\theta/2)}{\sqrt{m^2 - 2m\cos(\theta/2) + 1}} - \cos(\theta/2)\right)\Delta\theta \right| \tag{3}$$

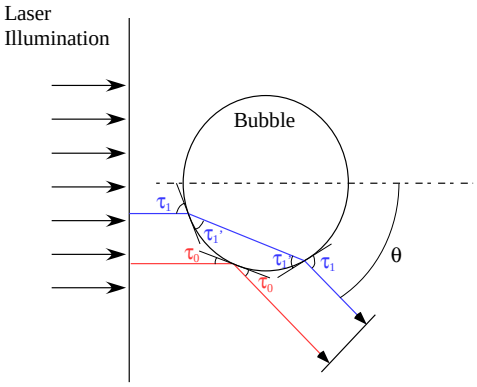

Figure 3: *Schematic of the optical pass of external reflection and refraction through the transparent spherical bubble in liquid.*

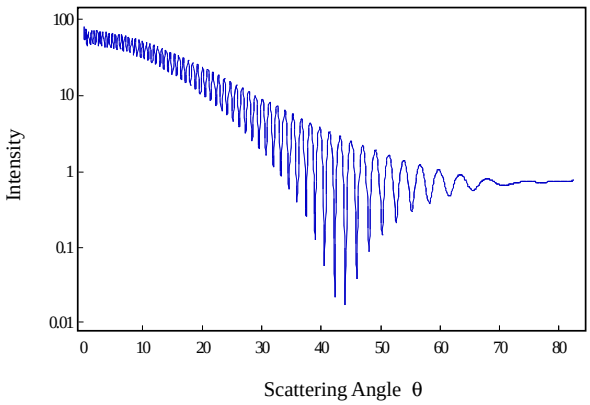

Figure 4: *The angular intensity profile scattered by the single bubble by laser light source at circular polarization .*

Recalling that the angular inter-fringe spacing is equal to 2π, Equation 3 can be rewritten by substituting $\alpha = N \times \Delta\theta$ as;

$$d = \frac{2\lambda N}{m\alpha} \cdot \frac{1}{\cos(\theta/2) - \dfrac{\sin(\theta/2)}{\sqrt{m^2 - 2m\cos(\theta/2) + 1}}} \tag{4}$$

where N is the number of fringes, α and θ is collecting and off-axis angle, respectively, of the receiving optics, m is the relative refractive index and λ is the wavelength of the light source. The geometry of this optical arrangement is shown in Figure 5. Equation 4 states the relation between the diameter of a single bubble and the number of fringes. The formulation for a spherical bubble, which is quite similar to that of droplets, shows that the diameter, d, is in direct proportion to the number of fringes, N. Equation 4 also states that the number of fringes, N, is independent of the light intensity of illumination.

Figure 6 shows the relation between the diameter of bubble and the number of fringes and its dependency on the collecting angle. It indicates the possibility of controlling the dynamic range and resolution of the measured diameter by adjusting the collecting angle, since a definite number of fringes can be counted on the receiving devices. i.e. a smaller collecting angle is suitable for a wide range of diameters, and a larger collecting angle is suitable for a narrow range with high accuracy. Figure 7 shows the relation between the off-axis angle and the number of fringes and indicates the angular limitation for the receiving optics.

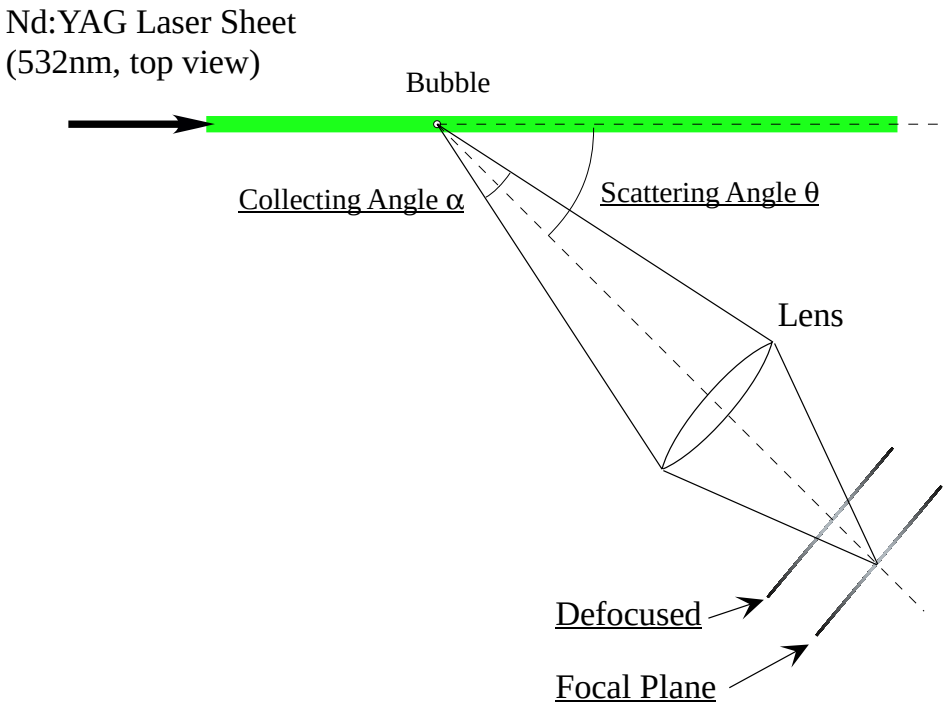

Figure 5: *Optical arrangement to observe focused and defocused plane.*

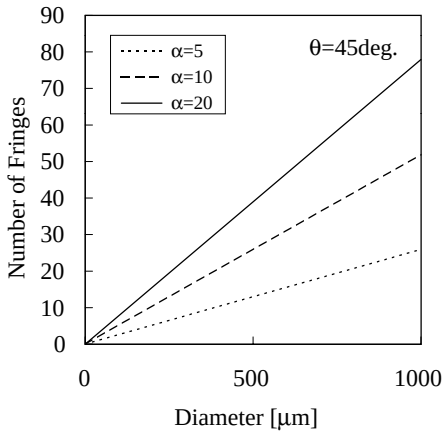

Figure 6: *Relation between the number of fringes and the bubble diameter.*

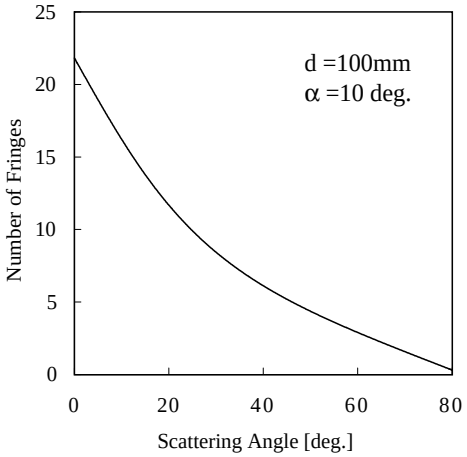

Figure 7: *Angular intensity profile from a single bubble by laser light source with circular polarization .*

2.2 Image processing method

a) Bubble sizing

Initially, the center positions of each bubble are extracted in order to distinguish each bubble before processing the frequency information. The template matching method with circular pattern can easily find the center of the circular fringe pattern from the array of bubbles, since there is no overlapping of the circular fringes in the captured picture when the number density of bubbles is low.

One of the great advantages of this interferometric technique is that the diameters of bubbles are obtained as frequency information, which indicates that the accuracy of measured diameters will be high compared with the intensity information. Figure 8 shows a brief example of a one-dimensional profile of the captured image by different bubbles which are the horizontal intensity distribution across the center of a circular fringe. The upper limitation of the measurable diameter range is determined by the maximum sampling frequency which is a function of the collecting angle and the magnification. The total number of sampling points, X, which is equal to 128 pixels in Figure 8, must be set appropriately in order to avoid both aliasing errors by discrete sampling and overlapping into the neighboring fringe by another bubble.

Many kinds of signal processing methods are available to analyze such frequency information as provided by Laser Doppler Velocimeter or Phase Doppler Anemometer, e.g. FFT method[Lading,1987; Lehman *et al.*,1988]. We adopted a spectral method based on the Gaussian fitting for peak determination with subpixel accuracy in the frequency domain[Maeda *et al.*, 1988; Kobashi *et al.*, 1990, 1992]. The discrete power spectrum essentially provides a broad distribution and it is difficult to find the peak, especially at the position of the middle point between the channels of fundamental frequency. If the real peak were the middle point of channels, the peak would be divided into two channels of almost the same height. This interpolation technique was carried out in order to improve the accuracy of the peak frequency of the signals and to enhance the resolution of the measured diameter.

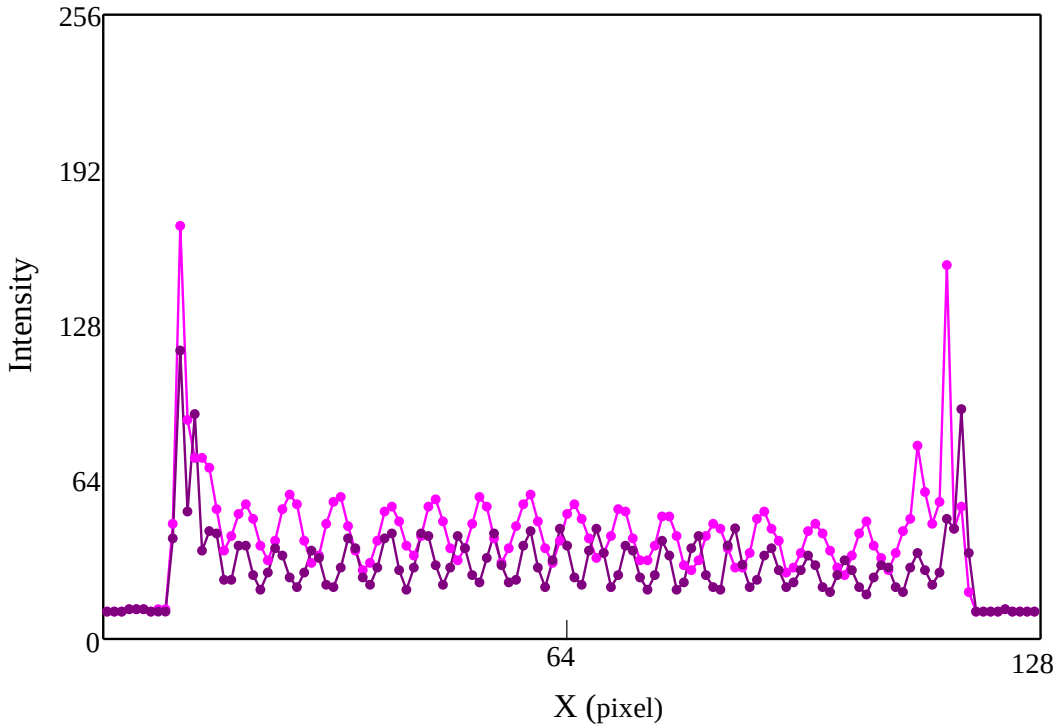

Figure 8: *An example of one-dimensional profile of captured fringe image by two different bubbles. High frequency(red line) is by larger bubble, low frequency(blue line) is by smaller one.*

Letting i and I represents the intensity signal of the fringe in real and frequency domain, respectively, P^2 is the power spectral density function written as;

$$I(\omega) = I_{re} + I_{im} = \int i(x)\, e^{j\omega x}\, dx \tag{5}$$

$$P(\omega) = \sqrt{I(\omega)\, I^*(\omega)} \tag{6}$$

Denoting k, the integer index of the peak frequency in the power spectrum, the modified frequency, f^*, using a Gaussian curve fitting is written as follows;

$$f^* = k + \frac{1}{2}\left(\frac{\log P_{k-1} - \log P_{k+1}}{\log P_{k-1} - 2\log P_k + \log P_{k+1}}\right) \tag{7}$$

The adjustment of Equation 7 remarkably reduces the bias error of the calculated frequency by less than 1% for the fundamental frequency. The bias error for absolute diameter is less than 0.02% while the error without the adjustment is 2%. This technique enables us to enhance the resolution of diameter from $10\mu m$ to approximately $0.1\mu m$ in our experimental configuration for a $500\mu m$ bubble.

b) Velocity determination

The rising velocity of the bubble is one of the most important parameters for characterizing the flow pattern of bubbly flow. The velocity of the single bubble can be obtained using the same concepts of the PIV or PTV techniques, i.e., to capture a couple of images with time interval δt as shown in Figure 9.

Here, $\delta s = (\delta x, \delta y)$ represents the displacement of the fringe images in the time interval, δt. The

velocity u is determined as follows;

$$u = \frac{\delta s}{\delta t} \tag{8}$$

δs was obtained by finding a similar pattern of two windows(sample0, sample1) within an interrogation window, i.e. the problem is the determination of the maximum value of the spatial cross correlation function.

When the time scale of the dissolution rate was much longer than that of rising movement, each pair of the fringe patterns in two instances should be the same and it allows us to obtain the displacement of a single bubble by the cross correlation method. In our experiment, the size of the reference windows were $128\ ^2\mathrm{pixels}$, which was enough to enclose one bubble. The width and height of the interrogation area were approximately $-10 \sim +10$ pixels, $-0 \sim +50$ pixels, respectively. Since the observed bubles were always rising within the stationary fluid, no bubbles went downward in our experimental conditions.

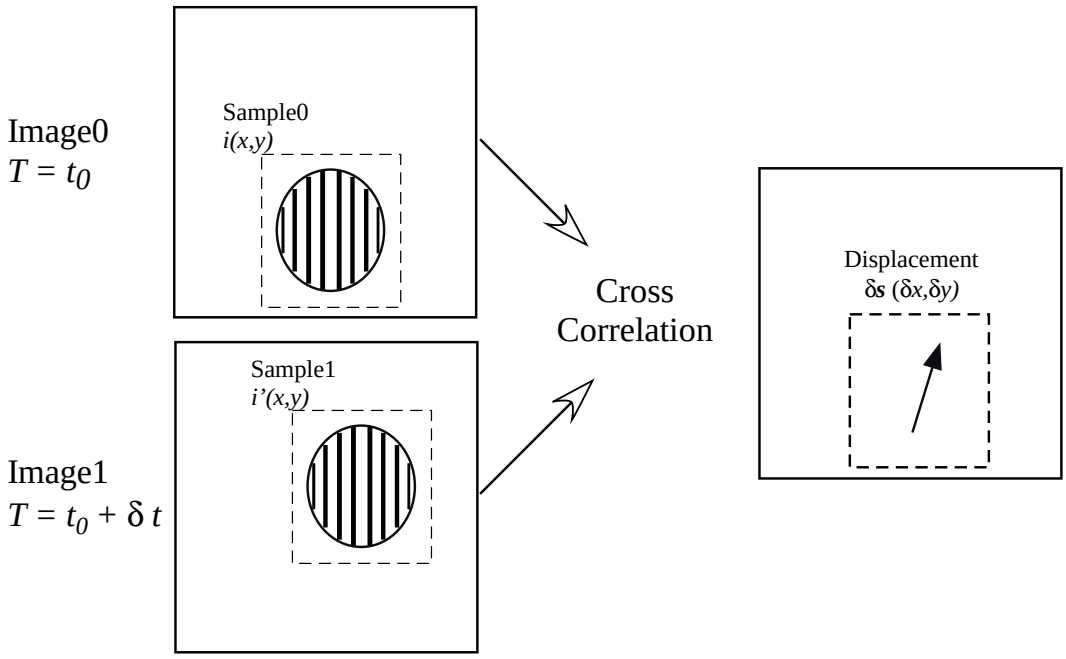

Figure 9: *Displacement estimation of a single bubble from a couple of double exposed images.*

3 Experiments and Results

A simplified depiction of the experimental apparatus was shown in Figure 2 in the Abstract. It consists of the degassed water tank with optical flat window on the laser pass, thin stainless injection nozzle of 100mm in length and $60\mu m$ internal diameter. The test section was located at the middle of the tank above the nozzle in order to observe the bubbles.

The optical equipment consisted of high power laser light and receiving optics. The laser source was a pulsed Nd:YAG laser at 532nm in wavelength, maximum power was 100mJ/pulse, repetition frequency was 30Hz in maximum, and the thickness of the laser sheet was $1500\mu m$ at the exhaust of the nozzle. The receiving devices were high resolution digital CCD cameras with 1k $\times$ 1k pixel resolution, each pixel has 10bit grayscale and the size of each pixel was $9\mu m^2$. The maximum size of the measuring area was $50\mathrm{mm}^2$ at most, and magnification in this geometry was 1:5. The distance of the objective lens and the bubbles in tank was set at 180mm so that the collecting angle would be $\alpha = 5^\circ$. The out-of-focus distance was 2.0mm from the focus plane.

At the beginning of our experiments, we performed a comparison of the proposed technique and the direct observing method by means of microscopic shadow imaging, and examined the results. The shadow images of air bubbles are captured by background illumination with an incoherent flash lamp. Captured images were processed into binary images in order to get the area of individual bubble. Since the shape of bubbles was completely spherical, the diameter, d, was calculated from the area a as $d = \sqrt{4a/\pi}$. From the result of our comparison study, the average diameter of bubbles by shadow imaging was $990\mu m$, and the bias error of the measured diameter by fringe method was less than 1% on average.

The gas dissolution experiment was done with pure gaseous CO_2, which is a dissolutive gas in water. The volume flux of CO_2 through the nozzle was $0.10 - 0.25\mathrm{mm}^3/\mathrm{s}$, the bubbles left the nozzle one by one in every 100 to 300ms. The takeoff of the bubble was not synchronized with the measurement system. Figure 10 is an instantaneous photograph of the fringe array of rising bubbles. We can easily find at least 8 circular fringe patterns in the picture, however, the real size of the bubbles was on the order of a hundred microns. Figure 11 shows the diameter transition of three bubbles by differing initial conditions. The maximum rate of the CO_2 dissolution was $0.20mm^3/s$ in volume for a $400\mu m$ bubble. Figure 12 shows the correlation between the diameter of bubble and its velocity. This map clearly shows that the rising velocities of larger bubbles are faster than those of smaller bubbles. The rising velocity in this diameter range is mainly determined by the buoyancy($\propto d^3$) and drag force($\propto d^2$), which is related to the surface condition including the presence of contamination by solid particles or dust or other, surfactants on the surface. In the present experimental arrangement, the measured range of velocity was 5 $\sim$ 30mm/s within the diameter range of 200 $\sim$ 400 μm .

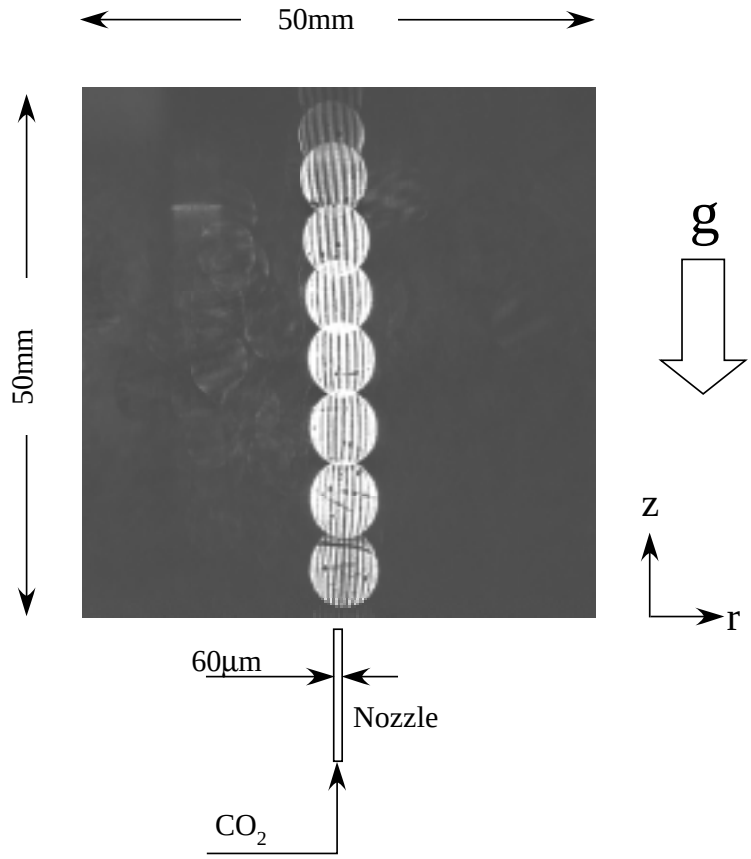

Figure 10: *The snapshot of the rising CO_2 bubble array, the range of diameter is approximately 240-300μm in this picture.*

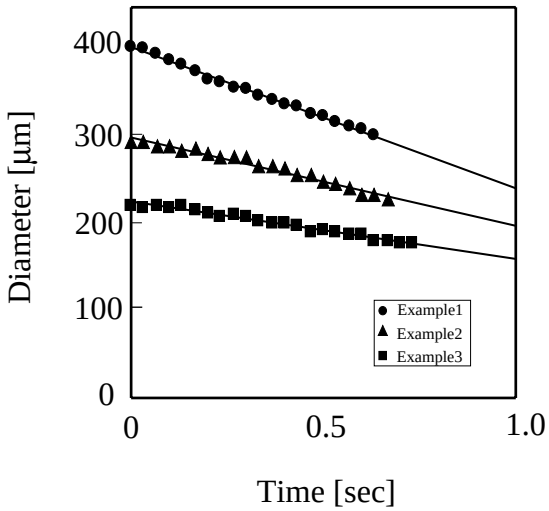

Figure 11: *Decrease of the diameter of three different bubbles as a function of time.*

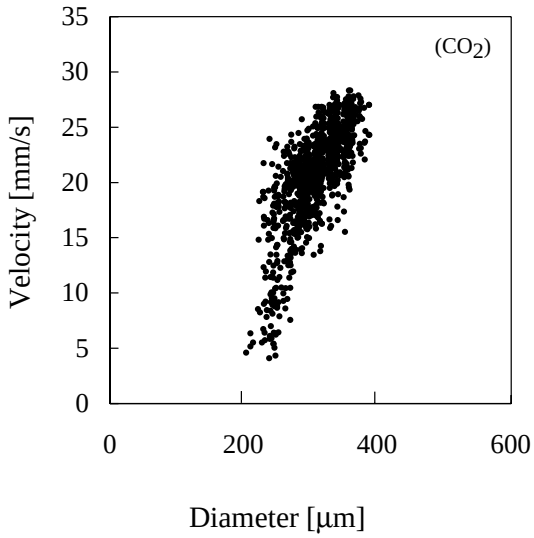

Figure 12: *Correlation of the diameter and rising velocity.*

4 Conclusions

1. An imaging technique for transparent spherical bubbles was developed based on the Mie Scattering Theory and ILIDS method. Considering the Geometrical optics we derived the relation between the bubble diameter and the number of fringes.

2. In order to process a large amount of data without any artificial bias, image processing logic for circular fringe images are constructed. [1] Find the location of bubbles with template matching method. [2] Count the number of individual fringes with an adjusted FFT method which gives the subpixel frequency information. [3] Calculate the inter-frame displacement of the circular fringe patterns by conventional cross-correlation method.

3. The experimental results of the CO_2 gas dissolution measurement by operating the high power pulsed laser source and high resolution digital CCD camera demonstrated that the proposed technique can provide time- and spatial-resolved information about the diameter and velocity for the individual spherical bubbles. The bias error of the measured diameter was less than 1% on average. The range of the measured velocity was $5 \sim 30$mm/s within the diameter range of $200 \sim 400$ μm for our experimental configuration.

Acknowledgement

This work was supported by a Grant-in-Aid of the Japanese Ministry of Education, Science and Culture (grant No. 11450078).

References

Bongiovanni,C., Chevaillier,J.Ph. and Fabre,J. (1997). "Sizing of Bubbles by Incoherent Imaging: Defocus Bias", Experiments in Fluids, 23, pp.209-216.

Brücker,Ch. (1998). "3-D Measurements of Bubble Motion and Wake Structure in Two-Phase Flows Using Scanning Particle Image Velocimetry (3-D SPIV) and Stereo Imaging", 9th Intl. Symp. on Appl. of Laser Tech. to Fluid Mech., 35-4.

Durst,F. and Zaré,M. (1975). "Laser Doppler Measurement in Two Phase Flows", Proceedings of LDA Symposium, pp.403-429.

Ford,B. and Loth,E. (2000). "Ellipsoidal bubble diffusion in a turbulent share layer", J. Multiphase Flow, 26, pp.503-516.

Giasole,T., Ren,K.F., Lebrun,D., Gouesbet,G. and Gréhan,G. (1998). "Particle Imaging Sizing: GLMT simulations", VSJ-SPIE98, AB0095.

Glover, A.R., Skippon, S.M. and Boyle, R.D. (1995). "Interferometric Laser Imaging for Droplet Sizing: A Method for Droplet-Size Measurement in Sparse Spray Systems", Applied Optics, Vol.34, No.36, pp.8409-8421.

Hess,C.F. (1998). "Planar Particle Image Analyzer", 9th Intl. Symp. on Appl. of Laser Tech. to Fluid Mech., 18-1.

Hirai,S., Okazaki,K., Yazawa,H., Ito,H., Tabe,Y. and Hijikata,K. (1997). "Measurement of CO_2 diffusion coefficient and application of LIF in pressurized water", Energy, Vol.22, No.2, pp.363-367.

Kobashi.K., Hishida,K. and Maeda,M. (1990). “Measurement of Fuel Injector Spray Flow of I.C. Engine by FFT Based Phase Doppler Anemometer - An Approach to the Time Series Measurement of Size and Velocity”, Applications of Laser Techniques to Fluid Mechanics, pp.268-287.

Kobashi,K., Hishida,K. and Maeda,M. (1992). “Multi-Purpose High Speed Signal Processor for LDA/PDA Using DSP Array”, 6th Intl. Symp. on Appl. of Laser Tech. to Fluid Mech., 21-6.

Lading,L. (1987). “Spectrum Analysis of LDA Signals”, ISL Proc. of an Intl. Specialists Meeting on the Use of Computers in Laser Velocimetry, 20-1.

Leman,B., Helbig,J and Simon,B. (1987). “A Software Processor Using FFT for Signal Burst Analysis in LDA”, ISL Proc. of an Intl. Specialists Meeting on the Use of Computers in Laser Velocimetry, 21.

Lin,S.M., Waterman,D.R. and Lettington,A.H. (2000). “Measurement of Droplet Velocity, Size and Refractive Index Using the Pulse Displacement Technique”, Meas. Sci. Technol., 11, L1-L4.

Maeda,M., Sanai,N., Kobashi,K. and Hishida,K. (1988). “Measurement of Spray Mist Flow by a Compact Fiber LDV and Doppler-Shift Detector with a Fast DSP”, 4th Intl. Symp. on Appl. of Laser Tech. to Fluid Mech., 6.8.

Morikita,H., Hishida,K. and Maeda,M. (1994). “Measurement of Size and Velocity of Arbitrarily Shaped Particles by LDA Based Shadow Image Technique”, Developments in Laser Techniques and Applications to Fluid Mechanics, pp.354-375.

Pajot,O. and Mounaïm-Rousselle,C (1998). “Droplet Sizing by Interferometric Method Based on Mie Scattering in an I.C. Engine”, 9th Intl. Symp. on Appl. of Laser Tech. to Fluid Mech., 18-2.

Roth,N., Andres,K. and Frohn,A. (1993). “Size and Evaporation Rate Measurements of Optically Levitated Droplets”, The Third Intl. Congress on Optical Particle Sizing, pp.371-377.

Schaller,J.K., Wassenberg,S., Fiedler,D.K. and Stojanoff,C.G. (1994). “A New Method for Temperature Measurements of Droplets”, ICLASS-94, 4-9 pp.443-450.

Van de Hulst,H.C. and Wang,R.T. (1991). “Glare Points”, Applied Optics, Vol.30, No.33, pp.4755-4763.